Thyroid hormone inactivation sustains cancer stem cell maintenance and tumorigenesis in basal cell carcinoma

Daniela Di Girolamo[1,2,11], Emery Di Cicco[3,4,11], Caterina Miro[3,11], Melania Murolo[3,5], Annarita Nappi[3], Annunziata Gaetana Cicatiello[3], Serena Sagliocchi[3], Lucia Acampora[3], Federica Restolfer[3], Jessica Ferraro[1], Stefano Sol[4], Fabiana Boncimino[4,6], Jovan Isma[4,7], Victor A. Neel[8], Tommaso Porcelli[9], Cedric Blainpain[10], Anna Mandinova[4] and Monica Dentice[2,3]

Journal of Investigative Dermatology (2026) ■, ■—■; doi:10.1016/j.jid.2026.01.025

A hierarchical organization within a tumor underlies the varying capacities of cancer cells to proliferate, metastasize, and drive relapse. Cancer stem cells (CSCs) are resistant to conventional therapies, making them critical targets for cancer treatment. Thyroid hormone (TH), a key regulator of proliferation and differentiation, is tightly controlled by the deiodinase enzymes. By integrating in vivo animal studies in a genetic mouse model of basal cell carcinoma (BCC) with analyses of human BCC specimens, we demonstrate that deiodinase type 3 (D3), the TH-inactivating enzyme, is expressed in the most tumorigenic CSC subpopulation. D3 genetic ablation significantly reduces the CSC population within protumorigenic niches and downregulates key stemness markers, including the transcription factor Sox9. Similarly, systemic induction of hyperthyroidism leads to a reduction of the CSC pool. Importantly, analysis of human BCC specimens revealed that D3 is highly enriched in the CSC niche. Mechanistically, we found that TH treatment suppresses Sox9 expression. These findings demonstrate that D3 sustains the tumorigenic potential of BCC CSCs by protecting them from TH-induced apoptosis and differentiation. Targeting the D3/TH axis may represent a promising therapeutic strategy to reduce the ability to self-renew of CSCs and inhibit tumor progression in BCC.

Keywords: Basal cell carcinoma, Cancer stem cells, Deiodinases, Thyroid hormone

INTRODUCTION

Basal cell carcinoma (BCC) accounts for ~80% of non-melanoma skin cancers and is the most common human malignancy worldwide (Rogers et al, 2015). UV-driven sequence alterations trigger and sustain the dysregulation of the Hedgehog pathway, through loss-of-function sequence variants in Ptch1, gain-of-function sequence variants in Smo, or overexpression of Gli1/2, playing a pivotal role in BCC development (Athar et al, 2006; Aszterbaum et al, 1999). Mouse models expressing oncogenic SmoM2 in the epidermis closely mimic human BCC and offer a valuable platform to investigate tumor initiation and progression (Blanpain and Simons, 2013; Mao et al, 2006; Youssef et al, 2010). Despite extensive insights into Hedgehog signaling, the cellular origin for BCC remains controversial. As for many other tissues, skin homeostasis and repair after injury are guaranteed by different types of stem cells (SCs) present in the epidermis (Blanpain and Fuchs, 2014). Owing to their long-term self-renewal ability, SCs have been hypothesized to serve as potential cells of origin for cancer. According to the hierarchical model, tumor growth is sustained by a minority population of highly tumorigenic cells, termed cancer SCs (CSCs) or tumor-initiating cells. Tumor-initiating cells possess stem-like self-renewal properties and upon cell division can give rise to both tumor-initiating cells and committed cells undergoing differentiation. This double program supports continued tumor expansion while preserving the ability to regenerate the full spectrum of tumor cell states (Pardal et al, 2003). However, identifying the specific SC populations responsible for initiating BCC has proven to be challenging, with several studies showing conflicting results (Youssef et al, 2012, 2010).

In mice, BCC preferentially arises from epidermal SCs in the interfollicular epidermis and infundibulum (Dlugosz, 1999; Youssef et al, 2012, 2010). Peterson et al (2015)

[1]Department of Biology, University of Naples Federico II, Naples, Italy; [2]CEINGE—Biotecnologie Avanzate Scarl, Naples, Italy; [3]Department of Clinical Medicine and Surgery, University of Naples Federico II, Naples, Italy; [4]Cutaneous Biology Research Center, Massachusetts General Hospital and Harvard Medical School, Charlestown, Massachusetts, USA; [5]Stem Cells and Development Unit, Institut Pasteur, Paris, France; [6]Department of Cellular, Computational and Integrative Biology (CIBIO), University of Trento, Trento, Italy; [7]Department of Immunobiology, University of Lausanne, Epalinges, Switzerland; [8]Department of Dermatology, Massachusetts General Hospital and Harvard Medical School, Boston, Massachusetts, USA; [9]Department of Public Health, University of Naples Federico II, Naples, Italy; and [10]Laboratory of Stem Cells and Cancer, Université Libre de Bruxelles (ULB), Brussels, Belgium

[11]These authors contributed equally to this work.

Correspondence: Monica Dentice, Department of Clinical Medicine and Surgery, University of Naples Federico II, Via S. Pansini, 5, Naples 80131, Italy. E-mail: monica.dentice@unina.it

Abbreviations: BCC, basal cell carcinoma; CFE, colony-forming efficiency; CSC, cancer stem cell; D2, type 2 iodothyronine deiodinase; D3, type 3 iodothyronine deiodinase; K, keratin; RT, room temperature; SC, stem cell; T3, triiodothyronine; T4, thyroxin; TH, thyroid hormone

Received 17 June 2025; revised 12 January 2026; accepted 14 January 2026; accepted manuscript published online XXX; corrected proof published online XXX

demonstrated that BCC arises preferentially from SCs within hair follicle and mechanosensory niches. Oncogenic Hedgehog pathway activation through SmoM2 expression or Ptch1 deletion driven by K14-CreERT in SCs but not in committed progenitors targeted by Inv-CreERT induces BCC formation (Sánchez-Danés et al, 2016). Other studies suggest that BCCs can also originate from keratin (K)15^{+}-bulge SCs, particularly in *Ptch1*$^{+/-}$ mice (Wang et al, 2011) or from both epidermal and bulge SCs upon Gli2 activation (Grachtchouk et al, 2011). These discrepancies likely reflect differences in genetic models and tumor subtypes because superficial and nodular BCCs may derive from distinct epidermal compartments.

Regardless of tumor origin, CSCs act as principal drivers of tumor growth, resistance, and metastasis. In BCC, the SC master regulator SOX9 is aberrantly reactivated, where it promotes cellular proliferation and suppresses keratinocyte differentiation (Larsimont et al, 2015). This reactivation orchestrates a gene network specific to cancer that bolsters stemness and cytoskeletal remodeling and reduces epidermal differentiation (Larsimont et al, 2015).

Thyroid hormone (TH) is an essential regulator of cellular proliferation, differentiation, and metabolism across diverse physiological contexts (Cicatiello et al, 2018; Miro et al, 2025b). Its precise intracellular availability is modulated by a family of iodothyronine deiodinases, which locally activate or inactivate TH (Gereben et al, 2008). In particular, type 3 iodothyronine deiodinase (D3) is the primary TH-inactivating enzyme, converting triiodothyronine (T3) into inactive metabolites and thereby terminating TH signaling. D3 is highly expressed during embryonic development (Dentice and Salvatore, 2011) but is largely absent in adult tissues, except for distinct sites such as the skin (Mancino et al, 2020). Loss of D3 in the adult epidermis resulted in significant tissue hypoplasia and increased differentiation of keratinocytes, indicating that D3 activity is required to maintain a proliferative, undifferentiated state in the epidermis (Mancino et al, 2020). Moreover, D3-deficient skin exhibited delayed wound healing and disrupted hair follicle cycling (Mancino et al, 2020). Notably, D3 is reactivated in pathological states characterized by heightened proliferation, including tissue regeneration and tumorigenesis (Dentice et al, 2012, 2009, 2007; Huang et al, 2000). In BCC, D3 is aberrantly expressed, resulting in localized TH inactivation in the tumor microenvironment. This creates a low-TH niche that promotes proliferation and impedes differentiation and apoptosis (Dentice et al, 2007; Luongo et al, 2014; Miro et al, 2017). Furthermore, keratinocyte-specific D3 ablation in a BCC mouse model sharply suppresses tumor growth, underscoring the pathological relevance of a regulatory axis involving the cancer-associated microRNA-21, the tumor suppressor gene GRHL3, and D3 (Di Girolamo et al, 2016).

In this study, we determined the role of D3 in the maintenance of the CSC pool of BCC. Using a mouse model of BCC, we found that D3 is expressed not only within the primary tumor but also in a specific CSC subpopulation with high CD34 expression (CD34^{Hi}) and robust tumor-forming ability. Importantly, D3 depletion led to a marked reduction in the CSC pool accompanied by downregulation of core stemness markers such as Sox9. Conversely, TH treatment, to mimic a hyperthyroid state, hindered CSC colony-forming ability and similarly diminished Sox9 expression. Importantly, analysis of human BCC samples revealed a significant enrichment of D3 within the SOX9-positive tumor niche. These results suggest that D3 supports the tumor-forming ability of BCC CSCs by shielding them from TH-induced differentiation, underscoring the therapeutic potential of targeting the D3/TH axis in BCC.

RESULTS

D3 maintains CSC identity and promotes BCC tumorigenesis

We previously demonstrated that D3 is essential for the maintenance of epidermal SCs by preserving their proliferative capacity and preventing premature differentiation (Mancino et al, 2020). In addition, we have shown that D3 is overexpressed in BCC under the regulation of the Shh signaling in a genetic mouse model in which BCC formation is driven by the overexpression of the oncogenic mutant SmoM2 specifically in the epidermis under the control of the K14-CreERT system (Canato et al, 2025; Dentice et al, 2007; Di Girolamo et al, 2016; Epstein, 2008; Luongo et al, 2014; Youssef et al, 2010). Overexpression of the Smo oncogene was induced by tamoxifen administration, and skin analysis was performed 8 weeks after induction. Consistent with our previous findings, we observed that D3 expression strongly correlates with BCC tumor formation in the tail, dorsal skin, and ear epidermis (Supplementary Figure S1a–d).

To assess whether D3 is expressed in CSCs, we used FACS to isolate the oncogene-expressing (SmoM2-YFP^{+}) basal cells (alpha-6-Integrin^{+}) CSCs (CD34^{+}) 8 weeks after tamoxifen administration in K14-CreERT/SmoM2-YFP mice (SmoD3WT) (Figure 1a and b). Because CD34 expression is critical for identifying the most protumorigenic niche of CSC in skin cancer (Canato et al, 2025; Lapouge et al, 2012; Malanchi et al, 2008), we measured D3 expression in FACS-isolated CD34^{Hi} cells, which exhibit high CD34 expression and a greater capacity to initiate tumors (Lapouge et al, 2012), and in CD34^{Lo} cells, characterized by an attenuated protumorigenic potential (Supplementary Figure S2a). Interestingly, D3 expression correlates with the CD34^{Hi} subpopulation, whereas type 2 iodothyronine deiodinase (D2), the TH-activating enzyme, is highly expressed in the CD34^{Lo} subpopulation (Figure 1c). These results show that the TH metabolism is finely regulated in CSCs, with a shift favoring inactivating deiodinase over activating one. This imbalance suggests that a hypothyroid-like state within the CSC niche may be essential for sustaining their protumorigenic and proliferative properties. Moreover, D3 did not colocalize with LGR5, thus pointing at D3 as a marker of the subpopulation of CD34^{+}, LGR5^{-} CSCs in BCC (Supplementary Figure S2b). In addition, we measured the expression of the TH receptor isoforms a and b (TRα and TRβ, encoded by the *THRA* and *THRB* genes) (Miro et al, 2023). When compared with the BCC tumor bulk, CSCs were characterized by a slightly lower expression of TRα and TRβ, thus confirming that CSCs are characterized by attenuated TH signal (high D3 and low D2, TRα and TRβ) (Supplementary Figure S2c).

To further define the role of D3 in the CSC niche, we depleted D3 in the epidermal compartment concomitantly

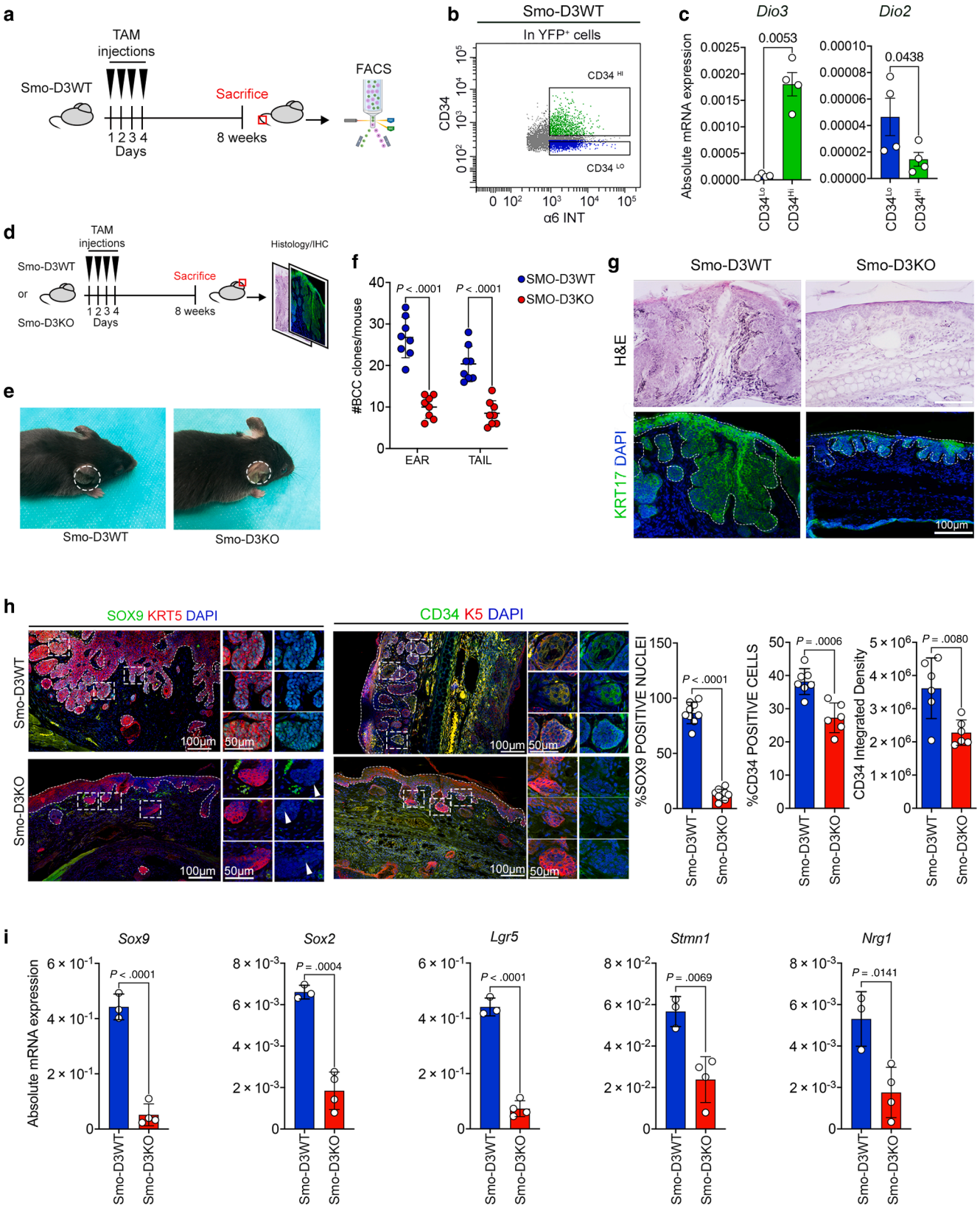

Figure 1. D3 regulates CSC identity and BCC tumor progression in mice. (**a**) Experimental workflow of BCC induction in mice; created with BioRender.com. **(b)** Single-cell suspensions were prepared from tail BCC-like lesions of Smo-D3WT (K14-CreERT; Smo-M2) mice, analyzed, and collected using a BD FACS Aria system. Cells were first gated for viability and singlets, followed by selection of YFP-positive (denoted as YFP^+) epithelial tumor cells. Within the YFP^+ population, CSC-enriched cells were identified on the basis of high expression of alpha-6-integrin (denoted as α6-INT) and CD34. Representative FACS plots show distinct separation of CD34 high ($CD34^{Hi}$, green) and CD34 low ($CD34^{Lo}$, blue) subpopulations within the α6-INT^+ compartment. The YFP^+/α6-INT^+/$CD34^{Hi}$ cells represent the CSC-like fraction and were used for downstream analyses; n = 4 mice. **(c)** RT-qPCR analysis of *Dio3* and *Dio2* expression in FACS-

with the induction of BCC formation driven by Smo overexpression. To this end, we crossed $D3^{fl/fl}$ mice (Dentice et al, 2014) with K14-CreERT/SmoM2 (Youssef et al, 2010) to specifically obtain D3 depletion and contextual Smo expression in the same cells (Smo-D3KO) after tamoxifen administration (Figure 1d). Efficient D3 depletion and Smo induction were confirmed by western blot and RT-PCR (Supplementary Figure S3a–c).

Compared with K14-CreERT/SmoM2; $D3^{WT/WT}$ mice (Smo-D3WT), K14-CreERT/SmoM2; $D3^{fl/fl}$ mice (Smo-D3KO) showed a reduced BCC formation (Figure 1e), number of tumors (Figure 1f), and a decreased expression of K5, typically overexpressed in tumor tissues (Aszterbaum et al, 1999; Markey et al, 1992) (Figure 1g and Supplementary Figure S4a). Conversely, the expression of K10, which has been reported to suppress tumor formation (Reichelt et al, 2004), was upregulated in Smo-D3KO mice (Supplementary Figure S4a). To assess whether D3 loss affects the stemness properties of SmoM2-expressing cells, we analyzed Sox9 expression, a key factor in maintaining the tumorigenic and proliferative potential of Smo-driven tumors (Kim et al, 2018; Lapouge et al, 2012; Larsimont et al, 2015). We found that Sox9-positive cells were significantly reduced in Smo-D3KO mice compared with those in Smo-D3WT mice (Figure 1h). Accordingly, Smo-D3KO BCC-like lesions were characterized by a global reduction of the expression of Shh signaling pathway compared with Smo-D3WT lesions, as demonstrated by the reduced mRNA levels of Gli1, Gli2, Gli3, Patch1, Ptch2, Nmyc1, and Dsvl2 (Supplementary Figure S4b). Immunofluorescence for CD34 further demonstrated that D3 depletion markedly diminished the number of $CD34^+$ cells (Figure 1h). Moreover, the remaining $CD34^+$ cells in Smo-D3KO mice displayed reduced fluorescence intensity compared with those in their Smo-D3WT mice counterparts (Figure 1h), indicating a loss of the $CD34^{Hi}$ CSC niche. Concurrently, RT-qPCR analysis demonstrated a significant downregulation of key stemness- and tumor cell plasticity–associated genes, including *Sox2*, *Nrg1*, *Lgr5*, *Stmn1*, and *Sox9* (Canato et al, 2025; Liao et al, 2022), in Smo-D3KO mice compared with those in Smo-D3WT controls (Figure 1i). Collectively, these findings demonstrate that D3 is essential for maintaining the self-renewal properties of the CSC niche in BCC.

TH regulates the abundance and phenotype of $CD34^+$ CSCs in BCC

To further assess the role of D3 in maintaining the CSC compartment in BCC, we performed FACS analysis to quantify $CD34^+$ cells within the SmoM2-YFP^+/alpha-6-$Integrin^+$ CSC population in Smo-D3WT and Smo-D3KO mice (Figure 2a). In Smo-D3WT mice, approximately 40% of SmoM2-YFP^+/alpha-6-$Integrin^+$ cells expressed CD34, whereas this percentage dropped to 10% in Smo-D3KO mice (Figure 2b and c). To clarify how D3 loss impacts the tumor-propagating potential of CSCs, we evaluated the distribution of $CD34^{Hi}$ and $CD34^{Lo}$ cells within the SmoM2-YFP^+/alpha-6-$Integrin^+$ population. Strikingly, Smo-D3KO mice showed a significant reduction in $CD34^{Hi}$ cells (from ∼85% to ∼60%) and a corresponding slight increase in $CD34^{Lo}$ cells, indicating that D3 is critical for sustaining the $CD34^{Hi}$ CSC niche (Figure 2d). Moreover, to investigate the role of TH signaling in this context, we treated Smo-D3KO mice with 0.1% methimazole, a compound that inhibits TH synthesis and reduces systemic TH levels (Azizi et al, 2019; Cooper, 1984), and 1% potassium perchlorate, which inhibits TH production by acting as a competitive inhibitor of iodine uptake in the thyroid gland, both administered through drinking water for 4 weeks after tamoxifen-induced tumor initiation (Figure 2e). Notably, methimazole treatment enhanced the tumor growth in Smo-D3KO mice, with a consequent increase in K17 and decrease in K10 (Figure 2f and g) and a partial restoration of $CD34^+$ cells compared with untreated Smo-D3KO controls and rescued the expression of Sox9 mRNA, indicating that systemic hypothyroidism promotes the expansion of protumorigenic CSCs (Figure 2h and Supplementary Figure S4c–e). Consistently with these data, administration of exogenous TH in Smo-D3WT mice, to mimic the hyperthyroid state resulting from D3 depletion (Figure 2i), led to a reduction of tumor growth (Figure 2j and k) and a significant reduction in the $CD34^{Hi}$ CSC population (Figure 2l and Supplementary Figure S4f and g), similarly to the upregulation of classical positive TH-target genes in the

isolated $CD34^{Hi}$ and $CD34^{Lo}$ CSC populations from mouse BCC-like lesions. Cells were isolated from the tail as described before. RT-qPCR was performed on RNA extracted from sorted $CD34^{Hi}$ and $CD34^{Lo}$ populations. Gene expression levels are shown as absolute values normalized to cyclophilin. n = 8 mice, with each data point representing a pool of cells from 2 mice. Data are presented as mean ± SD. Two-tailed unpaired *t*-test was performed. **(d)** Schematic representation of BCC induction in Smo-D3WT or Smo-D3KO mice and experimental workflow. **(e)** Representative images of mouse ears showing BCC lesions in Smo-D3WT (left) and Smo-D3KO (right) mice. The D3WT mouse displays a visibly greater tumor burden than the D3KO mice. Lesions are visible as raised, nodular lesions along the ear margin (area within the white line). Images are representative of at least n = 10 animals per genotype. **(f)** Quantification of BCC lesion number in Smo-D3WT versus Smo-D3KO mice. Scatter plots show the number of BCC clones per mouse in the ear and tail skin of Smo-D3WT (blue) and Smo-D3KO (red) mice. Each dot represents 1 mouse; data are presented as mean ± SD. Statistical significance was determined using an unpaired 2-tailed *t*-test. **(g)** Representative histological (H&E, top) and immunofluorescence (bottom) images of BCC-like lesions from Smo-D3WT and Smo-D3KO mice. H&E staining reveals extensive epithelial proliferation and dermal invasion in Smo-D3WT samples, whereas Smo-D3KO lesions exhibit reduced epithelial thickness and minimal invasion. Immunofluorescence staining for K17 (green), a marker of proliferating BCC epithelium, and DAPI (blue) highlights the diminished tumor architecture and epithelial outgrowths in D3-deficient tumors. Dashed lines delineate the epithelial–stromal boundary. Bar = 100 μm. **(h)** Representative immunofluorescence images of BCC-like lesions from Smo-D3WT and Smo-D3KO mice stained with anti-Sox9 and anti-K5 antibodies (left panels) or anti-CD34 and anti-K5 antibodies (right panels). Magnifications are indicated on the side of each image. Quantification includes the percentage of $Sox9^+$ cells per field, the percentage of $CD34^+$ cells per field, and the fluorescence intensity of CD34 staining per field, comparing Smo-D3WT with Smo-D3KO samples. Each data point represents 1 independent microscopic field. Quantification was performed using n = 4 mice per genotype. Data points shown represent pooled fields derived from all 4 mice within each genotype. **(i)** RT-qPCR analysis of the indicated stemness genes in SMO-D3 WT versus SMO-D3KO mice. Gene expression levels are shown as absolute values normalized to cyclophilin (n = 6 mice D3WT; n = 8 mice D3KO); each data point represents a pool of cells from 2 mice. Data are presented as mean ± SD. Two-tailed unpaired *t*-test was performed. BCC, basal cell carcinoma; CSC, cancer stem cell; D3, type 3 iodothyronine deiodinase; K17, keratin 17; K5, keratin 5.

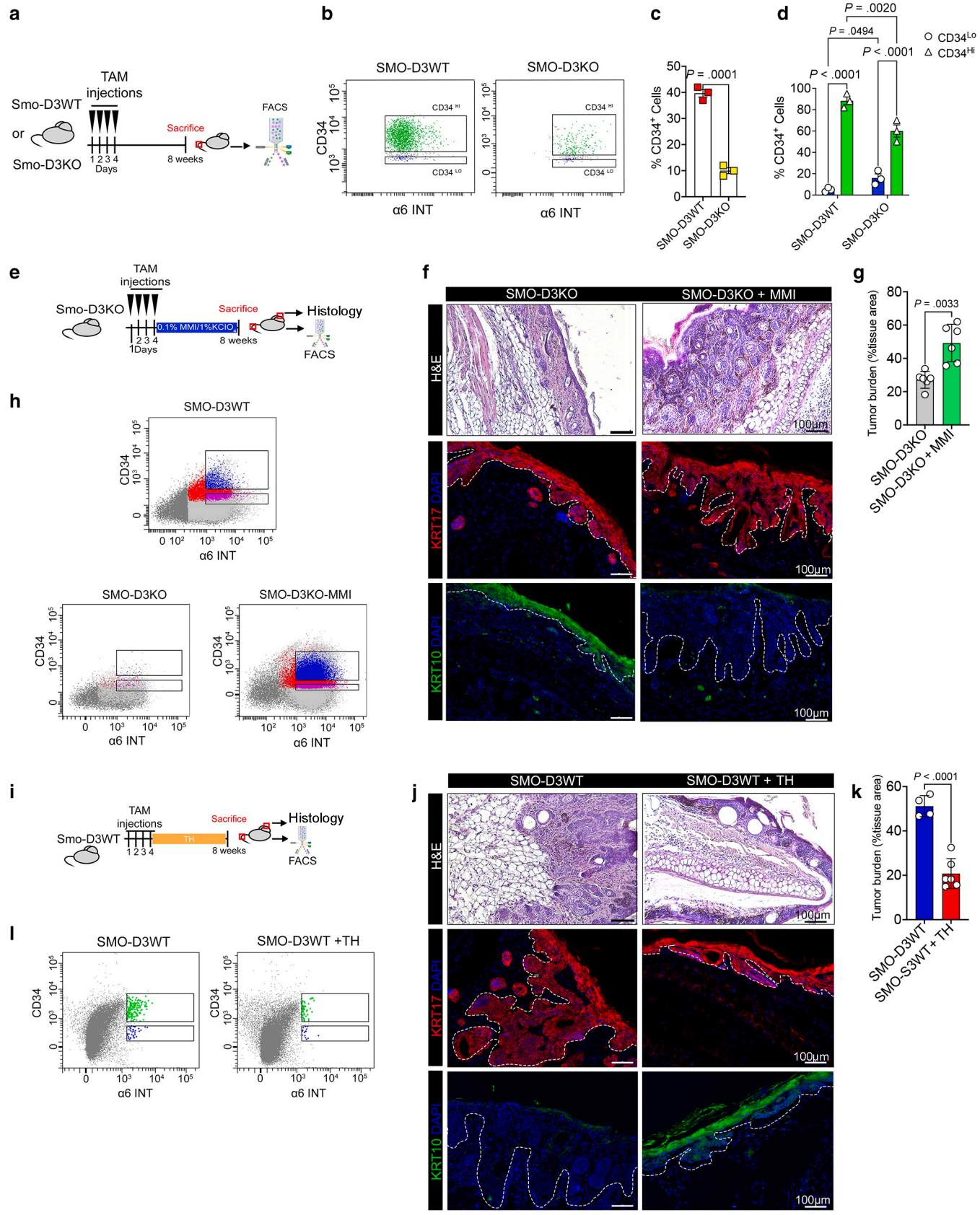

Figure 2. TH regulates CD34 CSCs population in BCC lesions. (**a**) Experimental workflow of BCC induction in Smo-D3WT or Smo-D3KO mice, created with BioRender.com. **(b)** Representative FACS plots showing the distinct separation of $CD34^{Hi}$ (green) and $CD34^{Lo}$ (blue) populations within the YFP^{+} and α6-$integrin^{+}$ epithelial tumor cells, gated as described in Figure 1b, from tail lesions of Smo-D3WT versus Smo-D3KO mice. Plots are representative of at least 3 independent experiments. **(c)** Quantification of the percentage of CD34-positive ($CD34^{+}$) cells analyzed with FACS analysis of tail lesions of Smo-D3WT versus

epidermis (*Krt 1* and *Krt 10*) and classical TH-negative target genes (*Krt5*, *Krt6*, and *Krt14*) (Mancino et al, 2021, 2020) (Supplementary Figure S5a). Altogether, these data support the conclusion that elevated TH levels impair CSCs self-renewal and niche maintenance.

TH suppresses BCC stemness by direct repression of Sox9

To investigate the direct effects of TH on BCC CSCs, we isolated the SmoM2-YFP^{+}/alpha-6-Integrin^{+}/CD34^{+} CSC population from Smo-D3WT mice by FACS. CD34^{+} CSCs were cultured in vitro in the presence or absence of exogenous TH (Figure 3a).

As shown in Figure 3b–d, in vitro exposure of Smo-D3WT CSCs to TH resulted in a strong reduction of their clonogenic potential. Specifically, TH treatment decreased colony-forming efficiency (CFE), the population-doubling capacity, and clone size compared with the control group, indicating a diminished self-renewal/proliferative capacity of CSCs upon TH exposure (Figure 3b–d). To determine whether this effect was also maintained in vivo, CSCs were isolated from Smo-D3WT mice treated systemically with TH and subsequently analyzed ex vivo (Figure 3e). Consistent with the in vitro data, CSCs from TH-treated Smo-D3WT mice displayed a drastic reduction in CFE compared with CSCs from untreated Smo-D3WT mice. Notably, CSCs isolated from Smo-D3KO mice exhibited a similarly low clonogenic capacity (Figure 3f). To further elucidate the underlying mechanisms, we examined the expression of Sox9 in the CSC colonies after TH treatment. Immunofluorescence analysis revealed a marked decrease in the number of Sox9-positive cells in the TH-treated group compared with that in the control group (Figure 3g [left panel] and h). In addition, the number of CD34^{+} cells within the same CSCs population treated with TH showed a reduction upon TH treatment (Figure 3g [right panel] and h.), suggesting that TH primarily impacts key SC markers in this short-term in vitro assay.

Because the main mode of action of TH is through the transcriptional regulation of target genes (Brent, 2012), we asked whether TH might inhibit *Sox9* expression. To this aim, we analyzed the *Sox9* regulatory region. In silico analysis revealed several conserved TH-responsive element binding sites within the mouse *Sox9* 5′-flanking regions (Figure 3i). We cloned 1241 bp of the 5′-flanking regions within the pGL3-basic vector to perform functional studies in mouse BCC cells.

As shown in Figure 3j, TH treatment significantly reduced the Sox9 promoter activity in the presence of TH receptors (TRα), compared with either the untreated condition (only TRα) or a generic promoter control (denoted as CMV). Chromatin immunoprecipitation assays on BCC cells treated with or without TH confirmed that TH treatment led to a significant decrease in TRα occupancy at the *Sox9* promoter, suggesting a direct transcriptional repression of *Sox9* by TH (Figure 3k). We also investigated whether, beside *Sox9*, genes belonging to the Shh signaling cascade might be regulated by TH in cultured CSCs. The expressions of *Gli1*, *Gli2*, and *Sox9* were repressed by 24 hours and 48 hours of TH treatment (Supplementary Figure S5b).

Collectively, these in vitro findings demonstrate that TH directly regulates BCC CSCs, at least partially, by binding to the *Sox9* promoter and reducing its expression and by reducing the Shh signal pathway.

D3 is enriched in the CSCs of human BCC

To attest that our results are translatable to human disease, we analyzed tissue specimens from patients with BCC (Figure 4a). We first confirmed the characteristic morphology of BCC in patient samples through histological analysis (Supplementary Figure S6a). To evaluate whether D3 contributes to the maintenance of the CSCs pool in human BCC lesions, we measured the expression levels of *DIO3* and several CSCs markers, including *SOX9*, *SOX2*, and *LGR5*, in BCC tissues compared with those in matched flanking skin from the same patients (normal skin) (Figure 4b). As expected, both *DIO3* and CSCs marker expressions were elevated in BCC relative to those in adjacent nontumoral skin (Figure 4b). We next performed immunofluorescence staining to assess the expression of D3 alongside key stemness markers within

Smo-D3KO mice. n = 6 mice per group, with each data point representing a pool of cells from 2 mice. Data are presented as mean ± SD. Unpaired *t*-test with Welch's correction was performed. **(d)** Quantification of the percentage of CD34^{Hi} (green) and CD34^{Lo} (blue) populations analyzed with FACS analysis of tail lesions of Smo-D3WT versus Smo-D3KO mice. n = 6 mice per group, with each data point representing a pool of cells from 2 mice. Data are presented as mean ± SD. Two-way ANOVA with uncorrected Fisher's LSD multiple comparison test was performed. **(e)** Experimental workflow of BCC induction in Smo-D3WT and Smo-D3KO mice, followed by treatment with 0.1% MMI and 1% $KClO_4$ administered for 4 weeks in drinking water to induce systemic hypothyroidism, created with BioRender.com. **(f)** Representative histologic and immunofluorescence analyses of skin from Smo−D3KO and Smo−D3KO + MMI mice. Top panels: H&E staining showing a reduction in epidermal thickening after MMI treatment. Middle panels: Immunofluorescence for K17 (red) and DAPI (blue) identifying basal-like, undifferentiated keratinocytes. Bottom panels: Immunofluorescence for K10 (green) and DAPI (blue) marking suprabasal differentiation. Dashed lines delineate the dermal−epidermal junction. Scale bars = 100 μm (**g**) Tumor burden expressed as percentage of total tissue area in Smo-D3KO mice treated with vehicle or MMI. Each dot represents an individual mouse. Bars indicate mean ± SD. Statistical significance was determined using an unpaired 2-tailed *t*-test with Welch's correction. **(h)** Representative FACS plots as previously described in Figure 1b, from tail lesions of Smo-D3WT; Smo-D3KO and Smo-D3KO mice treated with MMI as described earlier. Plots are representative of at least 3 independent experiments. **(i)** Experimental workflow of BCC induction in Smo-D3WT mice, followed by treatment with T3 and T4 (1.0 mg/ml T3 + 4.0 mg/ml T4) administered for 4 weeks in drinking water to induce systemic hyperthyroidism, created with BioRender.com. (**j**) Representative histologic and immunofluorescence analyses of skin from SMO-D3WT and SMO-WT + TH mice. Top panels: H&E staining showing a reduction in epidermal thickening after MMI treatment. Middle panels: Immunofluorescence for K17 (red) and DAPI (blue) identifying basal-like, undifferentiated keratinocytes. Bottom panels: Immunofluorescence for K10 (green) and DAPI (blue) marking suprabasal differentiation. Dashed lines delineate the dermal−epidermal junction. Scale bars = 100 μm **(k)** Tumor burden expressed as percentage of total tissue area in Smo-D3WT mice treated with vehicle or TH. Each dot represents an individual mouse. Bars indicate mean ± SD. Statistical significance was determined using an unpaired 2-tailed *t*-test with Welch's correction. (**l**) Representative FACS plots and quantification showing the distinct separation of CD34^{Hi} (green) and CD34^{Lo} (blue) populations within the CD34^{+} population of epithelial cancer tumor cells (gated as previously described), from tail lesions of Smo-D3WT and SMO-D3WT + TH. BCC, basal cell carcinoma; CSC, cancer stem cell; K10, keratin 10; K17, keratin 17; $KClO_4$, potassium perchlorate; LSD, least significant difference; MMI, methimazole; T3, triiodothyronine; T4, thyroxin; TH, thyroid hormone.

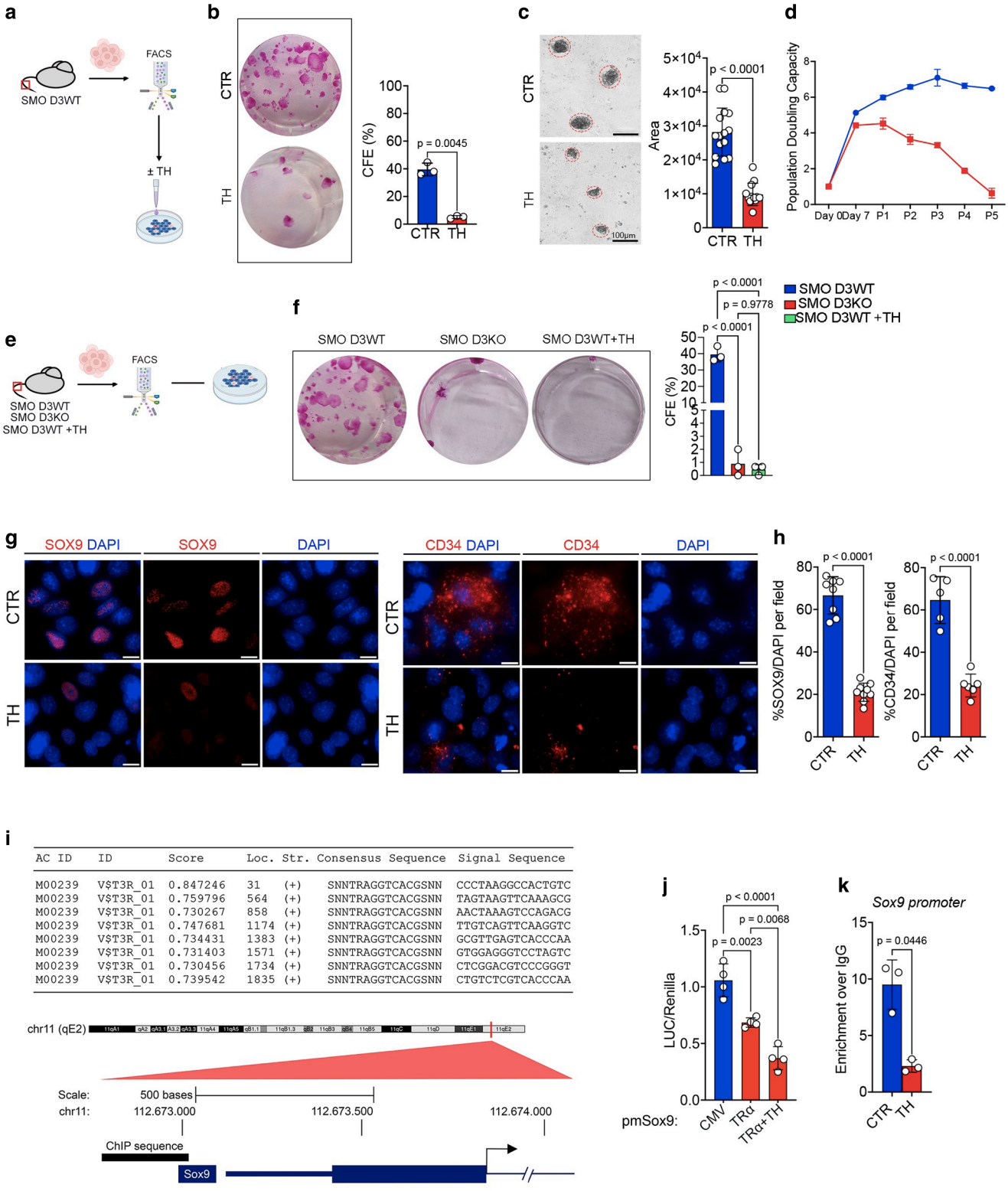

Figure 3. TH treatment suppresses SOX9 expression and self-renewal capacity in BCC-derived CSCs. (**a**) Experimental workflow for the isolation and in vitro culture of CSCs from mice with BCC, created with BioRender.com. **(b)** Representative images of CFE assays of CSCs cultured on mitotically inactivated 3T3-J2 feeder layers under control (denoted as CTR) conditions or treated with THs (30 nM T3 and 30 nM T4) for 12 days and stained with 2% rhodamine B. Quantification of CFE, calculated as (number of colonies / number of cells plated) × 100, shows a significant decrease in clonogenic potential upon TH treatment. Data represent mean ± SD; paired *t*-test was performed. (**c**) Representative brightfield images and quantification of colony formation from CSCs isolated from BCC lesions of Smo-D3WT mice. CSCs were sorted as $YFP^{+}/\alpha6\text{-integrin}^{+}/CD34^{Hi}$ cells and seeded in vitro. Cells were treated with vehicle (CTR) or TH (30 nM T3 and T4) for 5 days. Red circles indicate individual colonies. Bar graph shows quantification of colony area (μm^2). n = 3 biological replicates. Each data point represents an individual field. Data are presented as mean ± SD, analyzed with unpaired 2-tailed *t*-test. Bar = 300 μm. **(d)** PD of CSCs cultured on mitotically inactivated 3T3-J2 feeders with or without THs (30 nM T3/T4) up to passage 5. PD was calculated as $3.322 \times \log(N/N_0)$. Data represent mean ±

human BCC tissue, focusing on the relationship between D3 and SOX9. Immunofluorescence analysis revealed that cells with high SOX9 expression also exhibit elevated levels of D3, suggesting a potential role for D3 in supporting the transcriptional program associated with BCC stemness (Figure 4c). To further characterize the phenotype of D3-positive cells, we examined D3 expression in relation to the proliferation marker Ki-67. As previously shown (Kramer et al, 2014) within the D3-positive areas of human BCC lesions, numerous Ki-67−positive cells are present, confirming a positive association between D3 expression and cellular proliferation (Supplementary Figure S6b). To explore the specificity of this association, we examined D3 expression in relation to CD200, which identifies a tumor-initiating subpopulation in human BCCs (Colmont et al, 2013), and LGR5, a well-established marker of epithelial stemness (Jaks et al, 2008; Kostic et al, 2024; Sun et al, 2010). Interestingly, D3 expression correlated with CD200 (Figure 4d), whereas LGR5-positive BCC cells exhibited lower D3 fluorescence intensity, as also observed in mice (Supplementary Figure S2b), confirming that D3 defines a distinct subpopulation of stem-like BCCs that are not marked by LGR5 (Figure 4e). This conclusion is also supported by the analysis of published datasets indicating that D3 in human BCC colocalizes with numerous stemness markers (Supplementary Figures S7 and S8). Collectively, these findings suggest that in human BCC, D3 marks a distinct CSC population characterized by concurrent expression of the stemness markers CD200 and SOX9. This correlation supports the hypothesis that D3, by modulating local TH activity, contributes to the maintenance and self-renewal capacity of BCC stem-like cells, thereby promoting tumor growth and persistence.

DISCUSSION

Our study identifies type 3 deiodinase, D3, as a critical regulator of CSC identity and tumor progression in BCC. By integrating genetic mouse models, in vitro mechanistic assays, and analyses of human tumor specimens, we demonstrate that D3-driven modulation of local TH signaling is essential for sustaining the stemness and self-renewal capacity of the $CD34^{+}$ CSC niche in BCC.

TH controls many cellular processes in multiple cell types. Although TH concentrations in the blood are stable, the action of the deiodinases provides cell-specific regulation of TH activity (Ambrosio et al, 2013; Cicatiello et al, 2022; Luongo et al, 2019). Consequently, deregulation of deiodinase function and TH status has been implicated in tumorigenesis (Miro et al, 2025a; Nappi et al, 2025; Sagliocchi et al, 2023a, 2023b). We and others previously reported that D3 is overexpressed in the epidermis under Shh signaling and plays a key role in maintaining epidermal SC homeostasis (Dentice et al, 2007; Mancino et al, 2020). In detail, we observed that both TH treatment and D3 depletion affect normal keratinocyte growth and differentiation (Mancino et al, 2020). In addition, we expand on those findings by showing that D3 expression is markedly enriched in the $CD34^{Hi}$ subpopulation of CSCs, which represents the most protumorigenic compartment in murine BCC (Lapouge et al, 2012). In contrast, $CD34^{Lo}$ cells preferentially express D2, the TH-activating enzyme, suggesting that a tightly regulated TH gradient shapes distinct CSC states. Notably, D3 depletion in the epidermis significantly reduced BCC burden and led to a marked loss of the $CD34^{Hi}$ niche, accompanied by decreased expression of key stemness-associated markers such as *Sox9*, *Sox2*, and *Lgr5*. These findings support the concept that local hypothyroidism, enforced by D3, is required to maintain the tumor-propagating capacity of CSCs.

The data described earlier are in line with the previous report on the effects of D3-mediated TH clearance in colorectal CSCs (Catalano et al, 2016). Indeed, high levels of D3 expression correlated with β-catenin activation and enhanced self-renewal capacity of colorectal CSCs. Accordingly, it was demonstrated that loss of D3, by enhancing the TH signal, induced differentiation of colorectal CSCs and sensitized them to the standard chemotherapeutic drugs. Thus, along with these data, our work poises the evidence that D3 contributes to sustain the amplification of CSCs, in different tumor contexts, suggesting the use of deiodinase regulation as a tool with which to manipulate the CSCs fate and thus to modulate their expansion and differentiation in a therapeutic context. Strengthening this concept, in 3 tumor models of skin squamous cell carcinoma, colon cancer context, and prostate cancer, D3 was shown to be overexpressed in benign lesions with significantly higher levels than in normal tissues. However, its abundance negatively correlated with the histologic grade of the lesions, suggesting that D3 could be a marker of the early stages of tumorigenesis (Dentice et al, 2012; Miro et al, 2022, 2019).

SD (n = 3). **(e)** Schematic representation of the procedure used to isolate and culture CSCs from SMO-D3WT, SMO-D3KO, and SMO-D3KO + TH mice. Illustration was created with BioRender.com. **(f)** Representative images of CFE assays of CSCs isolated from SMO-D3WT, SMO-D3KO, and SMO-D3KO + TH mice, cultured on mitotically inactivated 3T3-J2 feeder layers for 12 days and stained with 2% rhodamine B. Quantification of CFE, calculated as (number of colonies / number of cells plated) × 100, shows significant differences in clonogenic potential among groups. Data represent mean ± SD, analyzed with 1-way ANOVA**. (g, h)** Representative images and quantification of immunofluorescence staining for SOX9 (red) (left panel) and CD34 (red) (right panel) of CSCs isolated as described earlier and treated with vehicle (denoted as CTR) or TH (30 nM T3 and T4) for 48 hours. n = 3 biological replicates. Each data point represents an individual field. data are presented as mean ± SD, analyzed with unpaired 2-tailed *t*-test. Bar = 10 μm. **(i)** In silico analysis identified multiple conserved TREs within the 5′-flanking region of the mouse *Sox9* gene. Scheme of the Sox9 locus on chromosome 11 with the predicted TRE sites and the region cloned for functional assays. The 1241 bp fragment upstream of the Sox9 transcription start site was inserted into a pGL3-basic luciferase reporter vector. **(j)** Luciferase reporter assays in mouse BCC cells (G2N2c) transfected with the *Sox9* promoter construct (*pmSox9*). Cells were treated with vehicle (CTR-CMV) or T3/T4 (TH, 30 nM) or cotransfected with TRα/β expression vectors (TRα), followed by T3/T4 treatment. TH treatment synergistically repressed *Sox9* promoter activity. Data are presented as mean ± SD; n = 4 biological replicates. One-way ANOVA with Šídák's multiple comparisons test was performed. **(k)** ChIP analysis of TRα binding to the *Sox9* promoter in G2N2c cells. Cells were treated with vehicle (CTR) or TH (30 nM T3 and T4) for 48 hours. ChIP was performed using an anti-TRα antibody or IgG control, and enrichment at the *Sox9* promoter was quantified by RT-qPCR. Data were normalized on input and shown as fold of enrichment over IgG. Bars represent mean ± SD. n = 3 biological replicates. Two-tailed paired *t*-test was performed. BCC, basal cell carcinoma; CFE, colony-forming efficiency; ChIP, chromatin immunoprecipitation; CSC, cancer stem cell; PD, population doubling; T3, triiodothyronine; T4, thyroxin; TH, thyroid hormone; TRE, thyroid hormone response element.

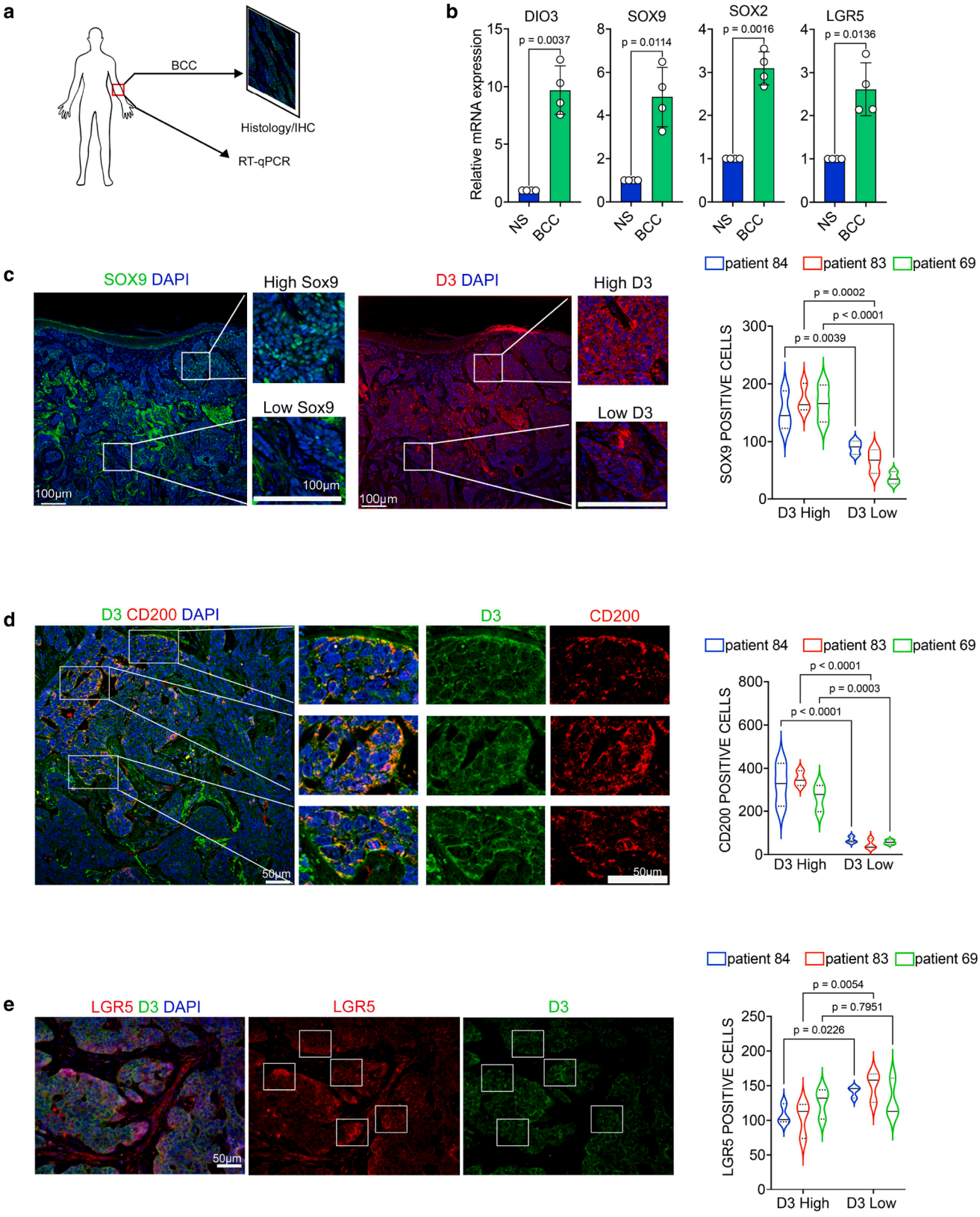

Figure 4. D3 expression correlates with cancer stem cell markers in human BCC lesions. (**a**) Experimental workflow for the human BCC samples analysis. **(b)** RT-qPCR analysis of the indicated genes in human BCC lesions compared with those in matched normal skin (denoted as NS) from the same patients. RNA was extracted from FFPE sections, and gene expression levels were normalized to *RPLP0* and expressed relative to NS. n = 4 patients. Data are presented as mean ± SD. Two-tailed paired *t*-test was performed. **(c)** Representative immunofluorescence images of human BCC tissue sections stained for SOX9 (green, left panel) and D3 (red, right panel) on sequential sections from the same patient. SOX9 displays nuclear localization, whereas D3 is predominantly membrane/cytoplasmic. Nuclei were counterstained with DAPI (blue). A magnified inset illustrates regions with high D3 signal spatially corresponding to areas enriched in SOX9^{+} nuclei, consistent with the quantification. Quantification shows the number of SOX9-positive nuclei in D3-high and D3-low cells, identified by D3

Our work further underscores functional importance of the TH-regulatory axis by manipulating systemic TH levels. Methimazole-induced hypothyroidism in D3-deficient mice rescued the CD34^{+} CSC pool, whereas exogenous TH administration mimicking the effects of D3 loss led to diminished CSC frequency, and as also observed in our previous works (Di Girolamo et al, 2016; Dentice et al, 2007; Luongo et al, 2014), TH reduced the expression of genes under the Shh signaling pathway. These in vivo experiments provide compelling evidence that the TH metabolic state governs CSC dynamics in BCC. Importantly, this regulation extends beyond cell abundance to include TH-dependent transcriptional repression of Sox9, a master regulator of epidermal stemness and proliferation. These results position Sox9 as a downstream effector of TH signaling, providing mechanistic insight into how elevated TH levels suppress CSC traits.

Previous studies have shown a similar repression of Sox2 expression by TH in non-neoplastic settings. In the neural SC niche of the subventricular zone, TH was found to regulate cellular plasticity and maintain homeostasis across mixed populations of SCs, transit-amplifying progenitors, and migrating neuroblasts (López-Juárez et al, 2012). In detail, TH and its receptor, TRα1, were directly involved in maintaining the balance between these cell populations by suppressing the Sox2^{+} cells (which give rise to oligodendrocytes) and favoring neural SC commitment toward a migrating neuroblast phenotype (López-Juárez et al, 2012). Taking these results together, the authors propose that the TH-dependent repression of Sox2 promotes differentiation of neural SC progenitors to a more committed phenotype.

The translational relevance of this work is underscored by our findings in human BCC specimens. Immunofluorescence analyses confirmed strong D3 expression in the tumor compartment, with clear colocalization with CD200 and SOX9. Interestingly, LGR5^{+} cells exhibited weaker D3 staining, indicating that D3 marks a distinct CSC subpopulation not fully overlapping with other epithelial SC markers. These data support a model in which D3-expressing CSCs represent a unique, transcriptionally defined niche dependent on local TH inactivation.

Collectively, our findings reveal a previously unrecognized role for TH metabolism in skin cancer stemness. Although D2 promotes the tumor progression in many tumor types and in the squamous cell carcinoma (Miro et al, 2022, 2019; Nappi et al, 2025; Sagliocchi et al, 2023a), the BCC, which has a low tendency to undergo metastasis, exhibits a different pattern of deiodinase expression, with high D3 and low D2 expression levels and a specific D3 signature in the CD34^{Hi} CSCs.

This work indicates that by lowering TH levels through D3 activity, BCC tumors maintain a prostemness, protumorigenic microenvironment that promotes CSCs persistence and tumor growth. These insights suggest that therapeutic strategies aimed at disrupting the D3−TH−SOX9 axis may effectively target the CSC niche and improve outcomes for patients with advanced BCC. Future studies will be needed to explore the efficacy and safety of systemic or local modulation of TH signaling in this context and to define whether this axis also operates in other skin cancers or epithelial malignancies as well as to address the effects of TH not only in the tumor bulk but also on the tumor microenvironment.

MATERIALS AND METHODS

Mouse strains

The K14-CreERT;SmoM2 mice (K14-CreER;Rosa26-LSL-SmoM2-YFP) were obtained from C. Blanpain laboratory. These mouse models are available at the Jackson Laboratory (stock number 005107 [https://www.jax.org/strain/005107] and stock number 005130 [https://www.jax.org/strain/005130]). SMO-D3KO mice (K14-CreERT;SmoM2,D3$^{fl/fl}$) were obtained by crossing the keratinocyte-specific conditional K14-CreERT mouse with D3$^{fl/fl}$ mice (Lapouge et al, 2012). Mice were fed regular chow ad libitum and maintained in fresh bedding cages under controlled conditions, namely 20−24°C, 50−60% humidity, and a 14:10 light−dark cycle. All animal experiments and mouse husbandry were done in the animal facility at CEINGE-Biotecnologie Avanzate (Naples, Italy). All in vivo procedures received the approval of the Institutional Animal Care and Use Committee (protocol number 1/2024-PR, D5A89.73).

Human specimens

Human samples were obtained from discarded skin specimens of BCC, alongside adjacent normal Skin at the Department of Dermatology, Massachusetts General Hospital (Boston, MA), with institutional approval (2018P003156).

Inducing oncogene activation and concomitant D3 genetic depletion

Male mice were induced at the age of 2 months with 10.0 mg of tamoxifen (tamoxifen-free base, Sigma-Aldrich, St. Louis, MO, code T5648) dissolved in 10% ethanol and 90% sunflower oil (Sigma-Aldrich, code C8267). Mice were treated with 4 consecutive intraperitoneal injections and killed 8 weeks after induction.

Induction of hypothyroidism in mice

Hypothyroid mice were obtained by treating Smo-D3WT and Smo-D3KO male mice aged 12 weeks with 0.1% methimazole (Sigma-Aldrich, code M8506) and 1% potassium perchlorate (Sigma-Aldrich, code 241830) mixed in drinking water for 4 weeks. Mice were killed 8

intensity thresholding. Data are shown as violin plots. n = 3 patients, n = 3 fields per sample. Data are presented as mean ± SD. Two-way ANOVA with Tukey's correction was performed. Scale bars = 100 μm **(d)** Representative immunofluorescence images of human BCC tissue sections stained for CD200 (red) and D3 (green). Nuclei were counterstained with DAPI (blue). Higher magnification illustrates the preferential association of CD200-positive cells with D3-high regions. Quantification shows the number of CD200-positive cells in D3-high and D3-low cells, identified by D3 intensity thresholding. Data are shown as violin plots. n = 3 patients, n = 3 fields per sample. Data are presented as mean ± SD. Two-way ANOVA with Tukey's correction was performed. Scale bars = 50 μm **(e)** Representative immunofluorescence images of human BCC tissue sections stained for LGR5 (red) and D3 (green). Nuclei were counterstained with DAPI (blue). A representative field at lower magnification shows that regions with high D3 expression correspond to areas with low LGR5 signal and vice versa, indicating an inverse spatial correlation between the 2 markers. Bars = 50 and 25 μm (left to right). Quantification of LGR5^{+} cells in D3-high and D3-low regions, defined by D3 intensity thresholding, is shown as violin plots. Data represent mean ± SD (n = 3 patients, 3 fields per sample). Statistical analysis was performed by 2-way ANOVA with Tukey's correction. BCC, basal cell carcinoma; D3, type 3 iodothyronine deiodinase; FFPE, formalin-fixed, paraffin-embedded.

weeks after tumor induction.

Induction of hyperthyroidism in mice

Hyperthyroid mice were obtained by treating K14-CreERT;SmoM2;D3WT male mice aged 12 weeks with T3 (1.0 mg/ml T3, Sigma-Aldrich, code T6397) and thyroxin (T4) (4.0 mg/ml T4, Sigma-Aldrich, code T2501) mixed in drinking water for 6 weeks (Cicatiello et al, 2022; Miro et al, 2023). Mice were killed 8 weeks after tumor induction.

Histology and immunostaining

For immunofluorescence and histology on mouse, tail, ear, or dorsal skin from K14-CreERT; SmoM2; D3WT and D3KO mice were embedded in paraffin, cut into 7.0-μm sections, and H&E stained. Slides were baked at 37 °C, deparaffinized by xylenes, dehydrated with ethanol, rehydrated in PBS, and permeabilized by placing them in 0.2% Triton X-100 in PBS. Antigens were retrieved by incubation in 0.1 M citrate buffer (pH 6.0) or 0.5 M Tris buffer (pH 8.0) at 95 °C for 5 minutes. Sections were blocked in 1% BSA/0.02% Tween/PBS for 1 hour at room temperature (RT). Primary antibodies were incubated overnight at 4 °C in blocking buffer and washed in 0.2% Tween/PBS. Secondary antibodies were incubated at RT for 1 hour and washed in 0.2% Tween/PBS. Images were acquired with a Leica DMi8 microscope and the Leica Application Suite LAS X Imaging Software (Leica Microsystems GmbH, Wetzlar, Germany, version 3.6.0.20104).

For immunofluorescence and histology on human BCC biopsies, images were obtained with a Yokogawa Spinning Disk Field Scanning Confocal System (Nikon) and analyzed with ImageJ (National Institutes of Health, Bethesda, MD).

The antibodies used for immunofluorescence analysis were anti-D3 (Novus Biological, Centennial, CO, code NBP1-05767), anti-CD34 (Proteintech Group, Rosemont, IL, code 60180-1), anti-LGR5 (Origene, Rockville, MD, code TA503316), anti-SOX9 (Abcam, Cambridge, United Kingdom, codes ab26414 and ab196450), anti-K17 (Novocastra Laboratories, Newcastle, United Kingdom, code NCL-CK17), anti-K10 (Covance, Princeton, NJ, code PRB-159P), and anti-K5 anticytokeratin/K5 (PROGEN Biotechnik GmbH, Wayne, PA, catalog number 03-GP-CK5).

Immunofluorescence on cells

Cells were fixed with 4% paraformaldehyde (Electron Microscopy Sciences) in PBS for 10 minutes at RT. Cells were washed 3 times in PBS, permeabilized in 0.5% Triton X-100 (Merck chemical, Sigma-Aldrich, code T8787) for 5 minutes RT, washed again 3 times in PBS, and blocked with 10% goat serum (Gibco, Thermo Fisher Scientific, Waltham, MA, code 16210072). Cells were incubated with the indicated primary antibodies overnight at 4 °C in PBS with 2% goat serum. Upon PBS washes, cells were incubated with secondary antibodies for 45 minutes at RT. DAPI (Invitrogen, Carlsbad, CA, catalog number D1306) was used to identify nuclei. All samples were mounted in 80% glycerol and covered with glass coverslips (number 1, VWR, Radnor, PA). Images were captured with a fluorescent Leica DMi8 microscope using the Leica Application Suite LAS X Imaging (Leica Microsystems GmbH, version 3.6.0.20104) for the acquisitions.

RNA extraction and real-time PCR

mRNAs were extracted with TRIzol reagent (Life Technologies, Carlsbad, CA, code 15596018). cDNAs were prepared with SuperScript VILO MasterMix (Life Technologies, code 11755-050) as indicated by the manufacturer. The cDNAs were amplified by PCR in a CFX Connect Real-Time PCR Detection System (Bio-Rad Laboratories, Hercules, CA, code 1855201) with the fluorescent double-stranded DNA-binding dye SYBR Green (Bio-Rad Laboratories, code 1708882). Specific primers for each gene were designed to work under the same cycling conditions (95 °C for 10 minutes followed by 40 cycles at 95 °C for 15 seconds and 60 °C for 1 minute), thereby generating products of comparable sizes (about 200–300 bp for each amplification). Primer combinations were positioned whenever possible to span an exon–exon junction, and the RNAs were digested with DNAse to avoid genomic DNA interference. For each reaction, standard curves for reference genes were constructed on the basis of six 4-fold serial dilutions of cDNA. All samples were run in triplicate. The template concentration was calculated from the cycle number when the amount of PCR product passed a threshold established in the exponential phase of the PCR. The relative amounts of gene expression were calculated with cyclophilin-A expression as an internal standard (calibrator). The results were expressed as $2^{(-\Delta Ct)}$. Primers used in this study are indicated in Table 1.

Protein extraction from skin and western blot analysis

Dorsal skin, ear, and tail were removed from mice and immediately snap frozen in liquid nitrogen. A total of 800 μl of lysis buffer (0.125 M Tris, pH 8.6; 3% SDS, protease inhibitors, including 1.0 mM phenylmethylsulfonyl fluoride and phosphatase inhibitors) were added to all dorsal skin samples, which were then homogenized with TissueLyser II (Qiagen, Hilden, Germany, code 85300). Total tissue protein was separated by 8–10 or 15% SDS-PAGE, accordingly to the protein size to analyze, followed by western blot. The membrane was then blocked with 5% nonfat dry milk (Bio-Rad Laboratories, code 1706404) in PBS-0.2% Tween. Primary antibodies for anti-D3 (717-homemade, 1:500, Novus Biological, code NBP1-05767, 1:1000) and antitubulin (Santa Cruz Biotechnology, Dallas, TX, code sc-5546, 1:10,000) were used overnight at 4 °C. The following secondary antibodies were also used: antimouse IgG-horseradish peroxidase (Bio-Rad Laboratories, code 1706516) and antirabbit IgG-horseradish peroxidase (Bio-Rad Laboratories, code 1706515) and detected by chemiluminescence using an ECL kit (Millipore, Burlington, MA, catalog number WBKLS0500). Tubulin was used as a loading control. All western blots were run in triplicate, and bands were quantified with ImageJ software (National Institutes of Health).

BCCs

BCCs (G2N2c) were derived from transgenic mice expressing a constitutively active form of GLI2 under the control of K5 promoter (Sheng et al, 2002), which generates BCC-like tumors called "trichoblastomas." BCCs were cultured under low calcium conditions with 8% calcium ion–chelated fetal bovine serum (HiMedia Leading BioSciences Company, Mumbai, India, code RM10432) and keratinocyte GF (Sigma-Aldrich, code K1757-10UG). All transient transfections for BCCs were performed using Lipofectamine 2000 (Invitrogen, catalog number 11668019), according to the manufacturer's instructions.

Luciferase assay

To generate the pmSox9Luc plasmid, we used a genomic mouse DNA as template in a PCR with oligonucleotides—pmSox9U (attaCTCGAGCCTAGAGCTTCGCCCTCTTAG) and pmSox9L2 (cggcAAGCTTctctcttgcaaagaaaagttc)—to isolate 1241 bp from the mouse Sox9 5′-flanking region. The amplified region was cloned into

Table 1. Oligonucleotides Used for Real-Time PCR

Gene	Forward Primer (5′→3′)	Reverse Primer (5′→3′)
CYCLOPHILIN A	AGTCCATCTATGGGGAGAAATTTG	GCCTCCACAATATTCATGCCTTC
DIO2	CTCTATGACTCGGTCATTCTGC	CTCTATGACTCGGTCATTCTGC
DIO3	CCTGGGACTCTGCTTCTGTAAC	GGGGTGTAAGAAAATGCTGTAGAG
MCT8	TTCGGCTGGGTGGTGGTGTTCGCT	ATCATACCCATCGCGAGGGCTC
MCT10	CAATAGTCAGCGTCTTCACAGACCT	GCAGCAGGATTGTGAAGACACTGC
TRα1	ACCACCGCAAACACAACATT	CATTCCGAGAAGCTGCTGTC
TRα2	AATGGTGGCTTGGGTGTGGT	CCTGAACAACATGCATTCCGA
TRβ	CACCGGGTATCACTACCGCTGT	CAGCACCAAGTCTGTTGCCATGC
HBEGF	AGACCCATGCCTCAGGAAAT	ACGACAGTACTACAGCCACC
KLK6	GGCGACATGAAAGAAGGCAA	ACAGCCACTTGTTTCTGAGG
TNFAIP2	CTTCCGTGGAGCAGAAATGG	GAAACAGTCCTGCAGCTCTG
NRG1	AACCCACCACCAGAGAATGT	GATGCTTTCTGTGTGCCCAT
NRP2	CTCCCACCAGAACTGTGAGT	GGCGTAGTCTGAGGTGAACT
SOX9	AGGGCTACGACTGGACGCTGGTG	TGTAATCGGGGTGGTCTTTCTTGTGCT
SOX2	CTACATGAACGGCTCGCCCACCTAC	CTGGCCTCGGACTTGACCACAGAG
TBX1	TGTCTCCCCGAGCCAGTGCGTT	GCTACCAAGAGCTGCCTCCACCTA
STMN1	AATCTGTCCCCGATTTCCCC	CCCGGTTCTCTTTGTTAGCC
LGR5	CAACATCAGTCAGCTACCCG	GTCTCAGCTGGTTGTTCTGC
SNF8	CCTGAGTTCCGAGTCCAGTT	CATTCCGATGTTTGAGGGCC
TGFA	CAACAAGTGCCCAGATTCCC	GATGGCTTGCTTCTTCTGGC
K16	GAAGATCCGGGACTGGTACC	AGCCTGGCATTGTCAATCTG

the Xho/HindIII sites of a pGL3-basic vector (Promega, Madison, WI). The pmSox9Luc plasmid and CMV-Renilla reporters were cotransfected into BCCs using Lipofectamine 2000 (Invitrogen, catalog number 11668019), according to the manufacturer's instructions. Luciferase activities were measured 48 hours after transfection using the Dual Luciferase Reporter Assay System (Promega, code E1910), and differences in transfection efficiency were corrected relative to the level of Renilla activity. Each construct was studied in triplicate in at least 3 separate transfection experiments.

Chromatin immunoprecipitation assay

Approximately 8×10^6 BCCs were fixed with 1% formaldehyde in growth medium at 37 °C for 30 minutes. Glycine was added to a final concentration of 0.125 M to stop crosslinking. Sonicated, cross-linked chromatin was centrifuged at 12,000 r.p.m. for 30 minutes to remove insoluble material. The soluble chromatin was diluted 10-fold in dilution buffer and used directly for chromatin immunoprecipitation assays. Five percent of total DNA was used as a positive control for PCR assays (denoted "input DNA"). Six optical density (A260) units of chromatin from BCCs were mixed with 10 µl (0.3 µg/µl) of anti-TRα and incubated at 4 °C for 3 hours before precipitation with protein A/G Sepharose (Sigma Chemical, GE Healthcare, code GE17-0780-01). After 5 rounds of washing, bound DNA–protein complexes were eluted by incubation with 1% SDS 0.1 M sodium bicarbonateelution buffer. Formaldehyde cross-links were reversed by incubation in 200 mM sodium chloride at 65 °C. Samples were extracted twice with phenol-chloroform and precipitated with ethanol. DNA fragments were recovered by centrifugation, resuspended in 50 µl of water, and used for real-time PCRs.

Flow cytometry, isolation, and culture of epithelial CSCs

Tail skin was removed from the mice and treated with trypsin 0.25% (Gibco, Thermo Fisher Scientific) at 4 °C overnight after removal of adipose tissue. The epidermal layer was separated from the dermis, chopped, and incubated with trypsin 0.25% for 7 minutes at 37 °C. After digestion, fetal bovine serum was added to the sample to inactivate trypsin. The cell suspension was then filtered twice with a 70-µM cell strainer (Corning, code CLS431751-50EA). Immunostaining was performed using allophycocyanin antimouse CD34 (BioLegend, San Diego, CA, code 119310) and phycoerythrin rat antihuman a6-Integrin (BD Pharmingen, code 555736) by incubation for 1 hour on ice. Living SmoM2-expressing epidermal cells were gated by forward scatter, side scatter, and expression of SmoM2-YFP. $YFP^+/\alpha6\text{-Integrin}^+/CD34^+$ cells were sorted using FACS Aria II (BD Biosciences) and analyzed immediately after isolation or cultured on mitomycin C (Sigma-Aldrich, code M4287)–treated feeder cells using 0.3 mM calcium chloride E-Medium as previously described (Novak and Fuchs, 2009) (DMEM without calcium/F12 3:1 [161965-026 and 31765-027, Gibco, Thermo Fisher Scientific], 15% chelex fetal bovine serum [Cha1115L, Cytivia], 0.4 µg/ml hydrocortisone [386698-25mg, Millipore], 5 µg/ml transferrin [Sigma-Aldrich, code T2252-100mg], 5 µg/ml insulin [Gibco, Thermo Fisher Scientific, code 12585-014], toxin cholera 10^{-10M} [Sigma-Aldrich, code C8052], 1% L-glutamine [Euroclone, Milan, Italy, code ECB3000D], 1% penicillin–streptomycin [ECB3001D, Euroclone], and 0.3% sodium bicarbonate [0.3 mM calcium chloride]).

CFE assay

The CFE assay was performed to assess the clonogenic potential of CSCs isolated from control mice and treated with 30 nM T3 and 30 nM T4. A total of 1000 cells were seeded on mitotically inactivated 3T3-J2 feeder layers and cultured under standard conditions as described earlier in the presence and absence of 30 nM T3 and 30 nM T4. Twelve days later, cells were fixed with 4% paraformaldehyde and stained with 2% rhodamine B. CFE values were

calculated using the following formula: CFE (%) = (number of colonies / number of cells plated) × 100.

Population doubling capacity

Proliferation potential was assessed to indicate the capacity of cells to produce cell generations. CSCs were continuously cultured on mitotically blocked 3T3-J2 feeder layer up to passage 5 in the presence and absence of 30 nM T3 and 30 nM T4. At each passage, cells were trypsinized and counted using trypan blue and cultured at a seeding density of 3000 cells/cm^2 for the next passage. The population doubling of cultured CSCs was calculated using the following equation:

$$PD = 3.322 \log N/N_0$$

where N is the number of harvested cells, and N_0 is the number of clonogenic cells.

Statistical analyses

The results are reported as means ± SD throughout the study. For experiments in which we compared 2 different conditions, Student's 2-tailed *t*-tests were applied. For the experiments in which multiple conditions were compared, we used 1-way or 2-way ANOVA with a multiple comparison test. In all experiments, differences were considered significant when $P < .05$. *P*-values are indicated in the figures.

ETHICS STATEMENT

All animal studies were conducted in compliance with institutional guidelines and national regulations for animal welfare and were approved by the local Institutional Animal Care and Use Committee of the University of Naples Federico II and conducted in accordance with institutional and national ethical guidelines (protocols 266/2025-PR and D5A89.98). All procedures were designed to minimize animal suffering. Human cutaneous basal cell carcinoma tissues were obtained from discarded surgical specimens provided by the Department of Dermatology, Massachusetts General Hospital (Boston, MA) under institutional review board approval (protocol 2018P003156).

DATA AVAILABILITY STATEMENT

The authors affirm that all data necessary for confirming the conclusions of the article are present within the article, figures, and tables.

ORCID

Monica Dentice: http://orcid.org/0000-0002-9977-3761

CONFLICT OF INTEREST

The authors state the following financial interests, which may be considered potential competing interests: AM is a cofounder (with equity) of New Frontier Bio, a consumer health company developing skincare and antiaging products, and has equity in DermBiont, a private company advancing targeted topical therapeutics for dermatologic indications. AM and SS receive research support from Shiseido. The remaining authors state no conflcit of interest.

ACKNOWLEDGMENTS

The authors gratefully acknowledge AIRC Foundation for Cancer Research in Italy for supporting Annarita Nappi (A.N.) by an AIRC Fellowship for Italy Post Doc grant − (project code 31215). This research was supported by grants awarded to Monica Dentice (M.D.) from AIRC Foundation for Cancer Research in Italy awarded to Monica Dentice (M.D.) (IG 29242) and Ministero dell'Istruzione, dell'Università e della Ricerca − MIUR (PRIN-2022 Grant, Project Code 2022HB54P9), and a grant awarded to Caterina Miro (C.M.) from AIRC Foundation for Cancer Research in Italy (MFAG 30433).

AUTHOR CONTRIBUTIONS

Conceptualization: DDG, EDC, CM, SSo, FB, AM, MD; Data Curation: DDG, EDC, CM, MM, AN, AGC, SSa, LA, FR, JF, SSo, FB, JI, TP, VAN; Formal Analysis: DDG, EDC, CM, MM, AN, AGC, SSa, LA, FR, JF, SSo, FB, JI, TP, VAN; Funding Acquisition: CM, AM, MD; Methodology: AM, CB, MD; Project Administration: MD; Resources: CM, AM, MD; Writing − Original Draft Preparation: DDG, ED, CM, MD

DECLARATION OF GENERATIVE ARTIFICIAL INTELLIGENCE (AI) OR LARGE LANGUAGE MODELS (LLMs)

ChatGPT (OpenAI) was used solely to assist with English language editing and clarity improvements in the preparation of the manuscript. No artificial intelligence tools were used for data analysis, experimental design, or interpretation of scientific results. The authors have reviewed the content generated by the AI/LLM and take responsibility for this content.

SUPPLEMENTARY MATERIAL

Supplementary material is linked to the online version of the paper at www.jidonline.org, and at 10.1016/j.jid.2026.01.025.

REFERENCES

Ambrosio R, Damiano V, Sibilio A, De Stefano MA, Avvedimento VE, Salvatore D, et al. Epigenetic control of type 2 and 3 deiodinases in myogenesis: role of lysine-specific demethylase enzyme and FoxO3. Nucleic Acids Res 2013;41:3551−62.

Aszterbaum M, Beech J, Epstein EH Jr. Ultraviolet radiation mutagenesis of hedgehog pathway genes in basal cell carcinomas. J Investig Dermatol Symp Proc 1999;4:41−5.

Athar M, Tang X, Lee JL, Kopelovich L, Kim AL. Hedgehog signalling in skin development and cancer. Exp Dermatol 2006;15:667−77.

Azizi F, Takyar M, Madreseh E, Amouzegar A. Treatment of toxic multinodular goiter: comparison of radioiodine and long-term methimazole treatment [published correction appears in Thyroid 2019;29:1871]. Thyroid 2019;29:625−30.

Blanpain C, Fuchs E. Stem cell plasticity. Plasticity of epithelial stem cells in tissue regeneration. Science 2014;344:1242281.

Blanpain C, Simons BD. Unravelling stem cell dynamics by lineage tracing. Nat Rev Mol Cell Biol 2013;14:489−502.

Brent GA. Mechanisms of thyroid hormone action. J Clin Invest 2012;122:3035−43.

Canato S, Sarate R, Carvalho-Marques S, Maia Soares R, Song Y, Monteiro-Ferreira S, et al. Survivin promotes stem cell competence for skin cancer initiation. Cancer Discov 2025;15:427−43.

Catalano V, Dentice M, Ambrosio R, Luongo C, Carollo R, Benfante A, et al. Activated thyroid hormone promotes differentiation and chemotherapeutic sensitization of colorectal cancer stem cells by regulating Wnt and BMP4 signaling. Cancer Res 2016;76:1237−44.

Cicatiello AG, Di Girolamo D, Dentice M. Metabolic effects of the intracellular regulation of thyroid hormone: old players, new concepts. Front Endocrinol (Lausanne) 2018;9:474.

Cicatiello AG, Sagliocchi S, Nappi A, Di Cicco E, Miro C, Murolo M, et al. Thyroid hormone regulates glutamine metabolism and anaplerotic fluxes by inducing mitochondrial glutamate aminotransferase GPT2 [published correction appears in Cell Rep 2022;38:110562] Cell Rep 2022;38:110409.

Colmont CS, Benketah A, Reed SH, Hawk NV, Telford WG, Ohyama M, et al. CD200-expressing human basal cell carcinoma cells initiate tumor growth. Proc Natl Acad Sci USA 2013;110:1434−9.

Cooper DS. Antithyroid drugs. N Engl J Med 1984;311:1353−62.

Dentice M, Ambrosio R, Damiano V, Sibilio A, Luongo C, Guardiola O, et al. Intracellular inactivation of thyroid hormone is a survival mechanism for muscle stem cell proliferation and lineage progression. Cell Metab 2014;20:1038−48.

Dentice M, Ambrosio R, Salvatore D. Role of type 3 deiodinase in cancer. Expert Opin Ther Targets 2009;13:1363−73.

Dentice M, Luongo C, Ambrosio R, Sibilio A, Casillo A, Iaccarino A, et al. β-catenin regulates deiodinase levels and thyroid hormone signaling in colon cancer cells. Gastroenterology 2012;143:1037−47.

Dentice M, Luongo C, Huang S, Ambrosio R, Elefante A, Mirebeau-Prunier D, et al. Sonic hedgehog-induced type 3 deiodinase blocks thyroid hormone action enhancing proliferation of normal and malignant keratinocytes. Proc Natl Acad Sci USA 2007;104:14466−71.

Dentice M, Salvatore D. Deiodinases: the balance of thyroid hormone: local impact of thyroid hormone inactivation. J Endocrinol 2011;209:273−82.

Di Girolamo D, Ambrosio R, De Stefano MA, Mancino G, Porcelli T, Luongo C, et al. Reciprocal interplay between thyroid hormone and microRNA-21 regulates hedgehog pathway-driven skin tumorigenesis. J Clin Invest 2016;126:2308–20.

Dlugosz A. The Hedgehog and the hair follicle: a growing relationship. J Clin Invest 1999;104:851–3.

Epstein EH. Basal cell carcinomas: attack of the hedgehog. Nat Rev Cancer 2008;8:743–54.

Gereben B, Zavacki AM, Ribich S, Kim BW, Huang SA, Simonides WS, et al. Cellular and molecular basis of deiodinase-regulated thyroid hormone signaling. Endocr Rev 2008;29:898–938.

Grachtchouk M, Pero J, Yang SH, Ermilov AN, Michael LE, Wang A, et al. Basal cell carcinomas in mice arise from hair follicle stem cells and multiple epithelial progenitor populations. J Clin Invest 2011;121:1768–81.

Huang SA, Tu HM, Harney JW, Venihaki M, Butte AJ, Kozakewich HP, et al. Severe hypothyroidism caused by type 3 iodothyronine deiodinase in infantile hemangiomas. N Engl J Med 2000;343:185–9.

Jaks V, Barker N, Kasper M, Van Es JH, Snippert HJ, Clevers H, et al. Lgr5 marks cycling, yet long-lived, hair follicle stem cells. Nat Genet 2008;40:1291–9.

Kim AL, Back JH, Chaudhary SC, Zhu Y, Athar M, Bickers DR. SOX9 transcriptionally regulates mTOR-induced proliferation of basal cell carcinomas. J Invest Dermatol 2018;138:1716–25.

Kostic L, Leung C, Ahmad Murad K, Kancheva S, Perna S, Lee B, et al. Lgr5 marks stem/progenitor cells contributing to epithelial and muscle development in the mouse esophagus. Nat Commun 2024;15:7145.

Kramer E, Herman O, Frand J, Leibou L, Spanier L, Vardy H. Ki67 as a biologic marker of basal cell carcinoma: a retrospective study. Isr Med Assoc J 2014;16:229–32.

Lapouge G, Beck B, Nassar D, Dubois C, Dekoninck S, Blanpain C. Skin squamous cell carcinoma propagating cells increase with tumour progression and invasiveness. EMBO J 2012;31:4563–75.

Larsimont JC, Youssef KK, Sánchez-Danés A, Sukumaran V, Defrance M, Delatte B, et al. Sox9 controls self-renewal of oncogene targeted cells and links tumor initiation and invasion. Cell Stem Cell 2015;17:60–73.

Liao G, Dai N, Xiong T, Wang L, Diao X, Xu Z, et al. Single-cell transcriptomics provides insights into the origin and microenvironment of human oesophageal high-grade intraepithelial neoplasia. Clin Transl Med 2022;12:e874.

López-Juárez A, Remaud S, Hassani Z, Jolivet P, Pierre Simons J, Sontag T, et al. Thyroid hormone signaling acts as a neurogenic switch by repressing Sox2 in the adult neural stem cell niche. Cell Stem Cell 2012;10:531–43.

Luongo C, Ambrosio R, Salzano S, Dlugosz AA, Missero C, Dentice M. The sonic hedgehog-induced type 3 deiodinase facilitates tumorigenesis of basal cell carcinoma by reducing Gli2 inactivation. Endocrinology 2014;155:2077–88.

Luongo C, Dentice M, Salvatore D. Deiodinases and their intricate role in thyroid hormone homeostasis. Nat Rev Endocrinol 2019;15:479–88.

Malanchi I, Peinado H, Kassen D, Hussenet T, Metzger D, Chambon P, et al. Cutaneous cancer stem cell maintenance is dependent on beta-catenin signalling. Nature 2008;452:650–3.

Mancino G, Miro C, Di Cicco E, Dentice M. Thyroid hormone action in epidermal development and homeostasis and its implications in the pathophysiology of the skin. J Endocrinol Invest 2021;44:1571–9.

Mancino G, Sibilio A, Luongo C, Di Cicco E, Miro C, Cicatiello AG, et al. The thyroid hormone inactivator enzyme, Type 3 deiodinase, is essential for coordination of keratinocyte growth and differentiation. Thyroid 2020;30:1066–78.

Mao J, Ligon KL, Rakhlin EY, Thayer SP, Bronson RT, Rowitch D, et al. A novel somatic mouse model to survey tumorigenic potential applied to the Hedgehog pathway. Cancer Res 2006;66:10171–8.

Markey AC, Lane EB, Macdonald DM, Leigh IM. Keratin expression in basal cell carcinomas. Br J Dermatol 1992;126:154–60.

Miro C, Ambrosio R, De Stefano MA, Di Girolamo D, Di Cicco E, Cicatiello AG, et al. The concerted action of Type 2 and Type 3 deiodinases regulates the cell cycle and survival of basal cell carcinoma cells. Thyroid 2017;27:567–76.

Miro C, Cicatiello AG, Dentice M, Nappi A. The role of deiodinases on metabolic alteration in cancer. Semin Cancer Biol 2025a;114:215–26.

Miro C, Cicatiello AG, Nappi A, Sagliocchi S, Acampora L, Restolfer F, et al. Leptin enhances the intracellular thyroid hormone activation in skeletal muscle to boost energy balance. Cell Metab 2025b;37:936–53.e7.

Miro C, Di Cicco E, Ambrosio R, Mancino G, Di Girolamo D, Cicatiello AG, et al. Thyroid hormone induces progression and invasiveness of squamous cell carcinomas by promoting a ZEB-1/E-cadherin switch. Nat Commun 2019;10:5410.

Miro C, Di Giovanni A, Murolo M, Cicatiello AG, Nappi A, Sagliocchi S, et al. Thyroid hormone and androgen signals mutually interplay and enhance inflammation and tumorigenic activation of tumor microenvironment in prostate cancer. Cancer Lett 2022;532:215581.

Miro C, Nappi A, Sagliocchi S, Di Cicco E, Murolo M, Torabinejad S, et al. Thyroid hormone regulates the lipid content of muscle fibers, thus affecting physical exercise performance. Int J Mol Sci 2023;24:12074.

Nappi A, Miro C, Cicatiello AG, Sagliocchi S, Acampora L, Restolfer F, et al. The thyroid hormone activating enzyme, DIO2, is a potential pan-cancer biomarker and immunotherapy target. J Endocrinol Invest 2025;48:1149–72.

Novak JA, Fuchs E. Methods Isolation and culture of epithelial stem cells. Biol 2009;482:215–32.

Pardal R, Clarke MF, Morrison SJ. Applying the principles of stem-cell biology to cancer. Nat Rev Cancer 2003;3:895–902.

Peterson SC, Eberl M, Vagnozzi AN, Belkadi A, Veniaminova NA, Verhaegen ME, et al. Basal cell carcinoma preferentially arises from stem cells within hair follicle and mechanosensory niches. Cell Stem Cell 2015;16:400–12.

Reichelt J, Furstenberger G, Magin TM. Loss of keratin 10 leads to mitogen-activated protein kinase (MAPK) activation, increased keratinocyte turnover, and decreased tumor formation in mice. J Invest Dermatol 2004;123:973–81.

Rogers HW, Weinstock MA, Feldman SR, Coldiron BM. Incidence estimate of nonmelanoma skin cancer (keratinocyte carcinomas) in the U.S. population, 2012. JAMA Dermatol 2015;151:1081–6.

Sagliocchi S, Acampora L, Cicatiello AG. Deiodination and tumor progression: the interplay between thyroid hormones intracellular activation and the androgen signal. J Basic Clin Physiol Pharmacol 2023a;34:551–3.

Sagliocchi S, Murolo M, Cicatiello AG, Miro C, Nappi A, Di Cicco E, et al. Repositioning of cefuroxime as novel selective inhibitor of the thyroid hormone activating enzyme type 2 deiodinase. Pharmacol Res 2023b;189:106685.

Sánchez-Danés A, Hannezo E, Larsimont JC, Liagre M, Youssef KK, Simons BD, et al. Defining the clonal dynamics leading to mouse skin tumour initiation. Nature 2016;536:298–303.

Sheng H, Goich S, Wang A, Grachtchouk M, Lowe L, MO R, et al. Dissecting the oncogenic potential of Gli2: deletion of an NH(2)-terminal fragment alters skin tumor phenotype. Cancer Res 2002;62:5308–16.

Sun G, Hasebe T, Fujimoto K, Lu R, Fu L, Matsuda H, et al. Spatio-temporal expression profile of stem cell-associated gene LGR5 in the intestine during thyroid hormone-dependent metamorphosis in Xenopus laevis. PLoS One 2010;5:e13605.

Wang GY, Wang J, Mancianti ML, Epstein EH Jr. Basal cell carcinomas arise from hair follicle stem cells in Ptch1(+/-) mice. Cancer Cell 2011;19:114–24.

Youssef KK, Lapouge G, Bouvrée K, Rorive S, Brohée S, Appelstein O, et al. Adult interfollicular tumour-initiating cells are reprogrammed into an embryonic hair follicle progenitor-like fate during basal cell carcinoma initiation. Nat Cell Biol 2012;14:1282–94.

Youssef KK, Van Keymeulen A, Lapouge G, Beck B, Michaux C, Achouri Y, et al. Identification of the cell lineage at the origin of basal cell carcinoma. Nat Cell Biol 2010;12:299–305.